The Astrophysical Journal, 739:12 (5pp), 2011 September 20 doi:10.1088/0004-637X/739/1/12

SEARCHING FOR WATER EARTHS IN THE NEAR-INFRARED

M. E. Zugger[1,2], J. F. Kasting[2,3], D. M. Williams[2,4], T. J. Kane[1,5], and C. R. Philbrick[6]
[1] Applied Research Laboratory, Pennsylvania State University, P.O. Box 30, State College, PA 16804, USA
[2] Center for Exoplanets and Habitable Worlds, The Pennsylvania State University, University Park, PA 16802, USA
[3] Department of Geosciences, 443 Deike Bldg., Penn State University, University Park, PA 16802, USA
[4] School of Science, Penn State Erie, The Behrend College, 4205 College Drive, Erie, PA 16563-0203, USA
[5] Department of Electrical Engineering, Penn State University, Electrical Engineering East, University Park, PA 16802, USA
[6] Physics Department, North Carolina State University, 432 Riddick Hall, Raleigh, NC 27695-8202, USA
Received 2011 May 6; accepted 2011 June 27; published 2011 August 29

ABSTRACT

Over 500 extrasolar planets (exoplanets) have now been discovered, but only a handful are small enough that they might be rocky terrestrial planets like Venus, Earth, and Mars. Recently, it has been proposed that observations of variability in scattered light (both polarized and total flux) from such terrestrial-sized exoplanets could be used to determine if they possess large surface oceans, an important indicator of potential habitability. Observing such oceans at visible wavelengths would be difficult, however, in part because of obscuration by atmospheric scattering. Here, we investigate whether observations performed in the near-infrared (NIR), where Rayleigh scattering is reduced, could improve the detectability of exoplanet oceans. We model two wavebands of the NIR which are "window regions" for an Earth-like atmosphere: 1.55–1.75 μm and 2.1–2.3 μm. Our model confirms that obscuration in these bands from Rayleigh scattering is very low, but aerosols are generally the limiting factor throughout the wavelength range for Earth-like atmospheres. As a result, observations at NIR wavelengths are significantly better at detecting oceans than those at visible wavelengths only when aerosols are very thin by Earth standards. Clouds further dilute the ocean reflection signature. Hence, other techniques, e.g., time-resolved color photometry, may be more effective in the search for liquid water on exoplanet surfaces. Observing an exo-Earth at NIR wavelengths does open the possibility of detecting water vapor or other absorbers in the atmosphere, by comparing scattered light in window regions to that in absorption bands.

Key words: methods: numerical – planets and satellites: atmospheres – planets and satellites: detection – planets and satellites: surfaces – polarization – radiative transfer

1. INTRODUCTION

1.1. Background

McCullough (2006), Williams & Gaidos (2008), Stam (2008), Robinson et al. (2010), and others have proposed that a large ocean could be detected on an extrasolar planet using orbital variations in brightness and polarization. Bailey (2007) suggested that liquid water clouds could be detected using a similar technique. Many of these authors also speculated that one could more easily detect such water signatures by observing at near-infrared (NIR) wavelengths, taking advantage of the λ^{-4} dependence of Rayleigh scattering. Also, molecular absorption bands for species of interest such as CO_2 and CH_4, and additional water vapor bands, occur in this range. A number of authors have considered the possibility of detecting broadband absorption spectra of transiting or front-illuminated terrestrial exoplanets, including biomarkers (Cockell et al. 2009; Des Marais et al. 2002; Ford et al. 2001; Kaltenegger et al. 2010; Kiang et al. 2007; Woolf et al. 2002) and in fact water vapor has been seen in broadband spectroscopy of transiting exoplanets (Barman 2007; Tinetti et al. 2007). Megapixel detector arrays capable of working at these wavelength ranges are now available for space applications. For example, the NIRCam instrument on the *James Webb Space Telescope* uses two different types of HgCdTe detectors to cover the 0.6–2.3 μm and 2.4–5.0 μm bands (Burriesci 2005; Hall et al. 2004). Large infrared detector arrays based on InSb are also available (Nesher et al. 2009). More recently, SiGe detector arrays have been developed for the 0.4–1.6 μm range (Sood et al. 2009). It is generally assumed that only a future space-based telescope would be capable of observing a terrestrial exoplanet, but it has been suggested that 50–100 m ground-based telescopes with advanced adaptive optics might also work for this purpose in the visible or NIR wavelengths (Angel 2003; Cavarroc & Boccaletti 2006; Gilmozzi 2004).

In a previous paper (Zugger et al. 2010) we developed a planetary radiative transfer model that includes both surface scattering and realistic Earth-like atmospheres. In that paper we primarily studied planet/star contrast ratios (a more useful parameterization of brightness) and polarization fractions from end-member planets observed in the wavelength range 0.5–1.0 μm. This wavelength range was chosen because it was the baseline wavelength range for the *Terrestrial Planet Finder-Coronograph* (*TPF-C*), a large space-based NASA telescope concept (Levine et al. 2006). A comparable planet-finding telescope is currently being considered for a future NASA flagship mission in the 2020–2030 timeframe.

In our previous paper we found that molecular absorption, aerosols, clouds, atmospheric and in-water Rayleigh scattering, and ocean waves all conspire to hide the characteristic signatures of ocean planets at visible wavelengths.

Here, we simulate polarized and unpolarized observations at longer NIR wavelengths of planets with ocean or desert surfaces. In particular, we chose the Earth atmospheric window bands at approximately 1.55–1.75 μm and 2.1–2.3 μm.[7] A planet-finding telescope like *TPF-C* will be positioned above Earth's atmosphere, but if we wish to observe oceans on Earth-like planets, then we need to be able to see through a similar

[7] There is another window for Earth-like atmospheres in the range 1.1–1.35 μm; model results in this range are similar to those in the 1.55–1.75 μm range, and so are not presented here.

atmosphere surrounding the exoplanet. Additional windows exist in Earth's atmosphere at longer wavelengths, but for wavelengths at and beyond 3 μm, thermal emission from the surface and atmosphere become significant, and would tend to obscure the ocean reflectance signatures we seek. It should be noted that a sufficiently smooth dielectric material such as liquid methane or flat, bare ice will reflect and polarize light in a way very similar to the way a liquid water surface does. The boiling points of water and methane differ by about 260 K at 1 atm, so approximate knowledge of the planet's orbit and atmosphere should allow us to distinguish these liquids. The preponderance of absorption bands due to hydrocarbons or water vapor in the atmosphere of such a planet would also be a strong indicator of the type of liquid beneath. However, distinguishing between water-covered and ice-covered planets could be difficult, if the ice surface is smooth and not covered with snow or dust.

In a complementary paper, Robinson et al. (2010) consider the detectability of ocean glint from Earth observed as if it were an extrasolar planet. Their model includes Earth geography, and a higher fidelity simulation of Earth-like clouds than ours does; their model also discusses the potential for the future *James Webb Space Telescope* to detect ocean glint on such an Earth twin, but does not consider polarization or atmospheric aerosols (haze).

1.2. Definitions, Assumptions, and Geometry of the Problem

The signatures we wish to model are maximized for edge-on orbits and are minimized or nonexistent for face-on orbits, so we confine this investigation to edge-on orbits. We seek to model Earth-like planets, so we assume an Earth-sized planet in a circular orbit 1 AU from a Sun-like G type star. We model end-member planets with a single surface type such as ocean or desert, so there is no variation with planet rotation. For a study of variation with rotation of Earth as an exoplanet, we refer the reader to Cowan et al. (2009), who showed that fractional land/ocean cover can be determined by time-resolved color photometry, given sufficient photons.

We follow the convention of Williams & Gaidos (2008) in using orbital longitude (OL) to indicate position in the orbit; OL is defined as 0° when the planet passes in front of the star (transit), 90° and 270° when the planet is displaced farthest from the star (quadrature), and 180° when the planet passes behind the star (secondary transit). For planets with a single surface type in a circular edge-on orbit, orbital light curves are symmetric such that the half orbit between OL = 0°–180° is a mirror image of the half orbit between OL = 180° and 360°; hence, we present graphs of only half the orbit, specifically the portion between OL = 0° and 180°. Polarized scattering from our model exoplanets is studied using polarization fraction, which is defined as the difference between the perpendicular and parallel components divided by their sum. The reference plane defining "perpendicular" and "parallel" is the scattering plane—which, for edge-on orbits, is identical to the plane of the orbit. For total (unpolarized) flux, we use the contrast ratio between the planet and the parent star, because this is one of the most important design considerations for a *TPF-C* class mission.

2. MODEL

Here, we summarize the model development and structure; more detail is provided in Zugger et al. (2010). The geometric aspects of light scattering from across the surface of a spherical planet in a circular orbit are handled by using a portion of the model from Williams & Gaidos (2008). To simulate scattering from the atmosphere and surface, we run a modified version of the 6SV code[8] (Kotchenova & Vermote 2007; Kotchenova et al. 2006). Radiative transfer in the atmosphere is simulated by solving the radiative transfer equation for each of the 30 layers. An Earth-like pressure and temperature profile is assumed. Linear polarization is incorporated by using the first three Stokes parameters (circular polarization is assumed to be negligible). Calculations are performed using 20 wavelengths between 0.25 and 4.0 μm and interpolating between them. Our water Earth and desert Earth models include atmospheric absorption, which is computed by 6SV for O_3, H_2O, O_2, CO_2, CH_4, and N_2O using statistical band models with a resolution of 10 cm^{-1}. The code assumes that all species except ozone and water vapor are well mixed; for these two species, Earth-like altitude profiles are used based on the 1962 U.S. Standard Atmosphere. (COESA 1962). Maritime aerosols (which consist primarily of saltwater droplets and salt crystals) are assumed for ocean surface cases, and desert aerosols are assumed for desert planets (D'Almeida et al. 1991; Lenoble & Brogniez 1984; Russell et al. 1996; Vermote et al. 2006). Light winds of 1.5 m s^{-1} are assumed for ocean surface cases. An exponential aerosol profile with a scale height of 2 km is assumed; details of the aerosol distribution depend on the type of aerosol and visibility selected.

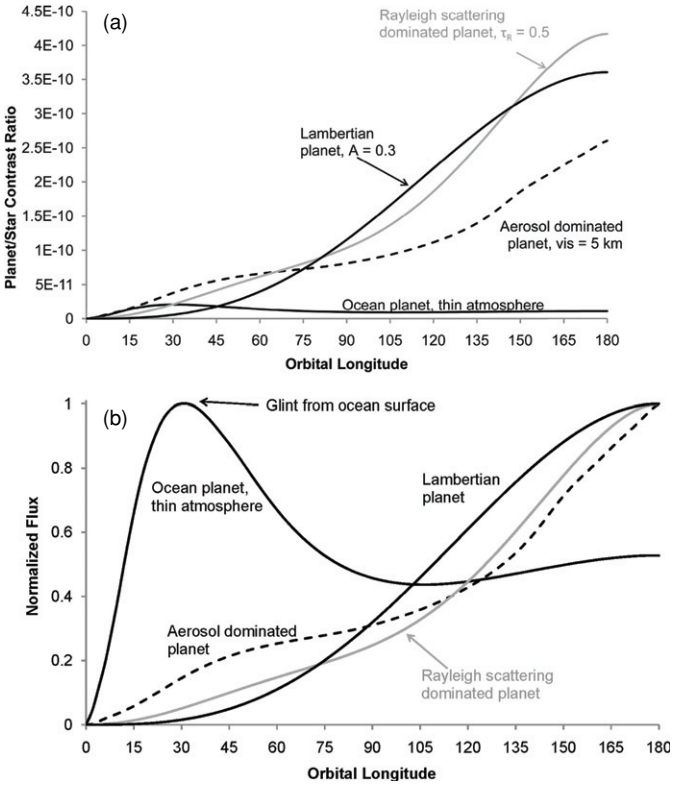

Figure 1. Contrast ratio (a) and normalized flux curves (b) from four end-member planet types; ocean planets with thin atmospheres and without clouds are comparatively dim, but glint from a liquid surface has a distinctive peak near OL = 30°.

3. RESULTS

In Figures 1(a) and (b), we compare the normalized unpolarized light curves from four end-member planets, specifically, (1)

[8] 6SV stands for Second Simulation of a Satellite Signal in the Solar Spectrum–Vector. A user's manual and a version of the Fortran code are available for download at http://6s.ltdri.org/.

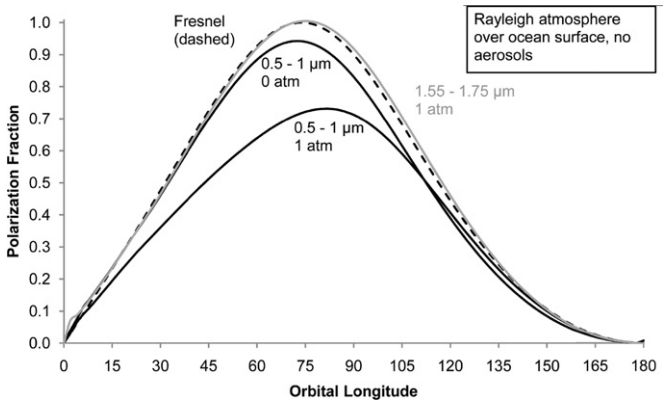

Figure 2. Polarization fraction of a water planet with Earth-like Rayleigh scattering atmosphere observed at two different wavebands; the NIR band removes dilution by atmospheric and in-water Rayleigh scattering, so the NIR curve falls almost on top of the analytical Fresnel result.

a Lambertian planet, dominated by diffuse surface reflectance; (2) an ocean planet, dominated by ocean surface glint; (3) a planet on which atmospheric Rayleigh scattering dominates; and (4) a planet dominated by atmospheric water aerosols. Clouds are neglected. The Lambertian planet is modeled using a reflectance that drops off with the cosine of the view angle; here, we assume a Bond albedo of 0.3, similar to that of the Earth (although the Earth is far from Lambertian). For the ocean planet, a negligible atmosphere is assumed, although a real water planet will naturally have at least a thin atmosphere and some water aerosols. The ocean planet curves were generated using the 0.5–1.0 μm band, but without an atmosphere, curves at the other wavebands differ only slightly. The Rayleigh dominated planet assumes a dark surface and a Rayleigh-scattering depth of $\tau_R = 0.5$. The aerosol-dominated planet assumes oceanic aerosols with a visibility of 5 km over a calm ocean surface.

In Figure 1(a), we plot the planet/star contrast ratios of each of the four end-member planet types. The magnitudes of such curves vary somewhat with the values of the parameters listed above, but the ocean planet (provided it has a thin atmosphere and minimal clouds) is significantly dimmer than the others. This fact could be diagnostic but may also hinder detection of some planets of this type. Figure 1(b) shows the same curves as Figure 1(a) but normalized to a peak brightness of unity to highlight the shapes of the curves. For these simplified cases the ocean planet with a thin atmosphere is easily distinguishable from the other cases because of the brightness peak in the crescent phase near OL = 30°.

In Figure 2, we compare the polarization fraction predicted by Fresnel's equations from an air/water boundary (dashed curve) against model predictions for ocean planets with Earth-like absorption and Rayleigh scattering atmospheres, but no aerosols. The model predictions for the *TPF-C* waveband for 0 and 1 bar atmospheres from Zugger et al. (2010) are shown along with the curve for the 1.55–1.75 μm waveband with a 1 bar atmosphere. The no-atmosphere case has a peak polarization fraction of 0.9; the polarization fraction is less than one and is shifted to about OL = 71°, as a result of dilution by scattering within the water column. The curve for the *TPF-C* waveband case with a 1 bar atmosphere is shifted by atmospheric Rayleigh scattering to peak at 83°, closer to the Rayleigh peak at 90° than to the Fresnel water surface peak at 74°. However, observing in the 1.55–1.75 μm waveband almost completely removes the effects of Rayleigh scattering from the polarization fraction

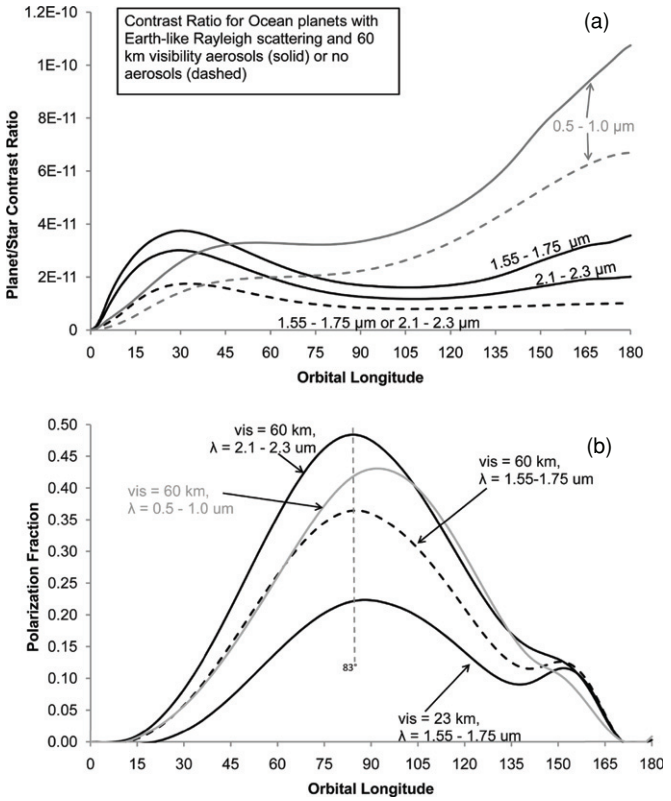

Figure 3. Contrast ratio (a) and polarization fraction (b) for water Earths with very thin 60 km visibility aerosols or no aerosols; moving to longer wavelengths essentially removes the effects of Rayleigh scattering and allows the water polarization peak to be detected if the aerosols are very thin.

curve, so the resulting NIR polarization curve falls almost exactly on the Fresnel curve for an air/water interface.

Figure 2 supports predictions that observing at longer wavelengths can remove the obscuration of an ocean's polarization signature by Rayleigh scattering. However, real atmospheres on ocean planets will contain at least some aerosols and water vapor absorption; therefore, the question is, what happens to the polarization fraction and contrast ratio when aerosols are included? Figure 3 shows (a) contrast ratios and (b) polarization fractions for water Earth planets with Earth-like absorption and maritime aerosols. Here, we chose aerosols that allow 60 km visibility, extremely thin aerosols by Earth standards; for comparison, 23 km visibility is the standard visibility for a clear day on Earth (McClatchey et al. 1972).[9] Dashed curves represent contrast ratios for cases without aerosols. (Earth-like absorption is also included, but has little effect in these chosen window regions.) We find that contrast ratios are dominated by aerosols, even for these thin aerosol cases. On the polarization fraction curves (Figure 3(b)) the 0.5–1.0 μm band peaks at just over 90°, again concealing any evidence of the ocean glint peak at 74°. However, the polarization fraction curves in the NIR windows peak near 83°, far enough from the Rayleigh peak at 90° to suggest that a water surface may lie beneath.

[9] Table 3 of McClatchey et al. (1972) provides particle number densities versus altitude for the 23 km visibility "clear" atmosphere and the 5 km visibility "hazy" atmosphere. The visibilities referred to are horizontal visibility at ground level at 550 nm. Vermote et al. (2006), p. 128, states that the vertical optical thickness of a 23 km visibility aerosol atmosphere is 0.235, and for a 50 km visibility aerosol, 0.152. Subroutines AEROSO, MIE, and ODA550 of 6SV calculate the scattering by aerosols based on the type and visibility of aerosols selected, and are described in Vermote et al. (2006), pp. 87–90 and 108–129.

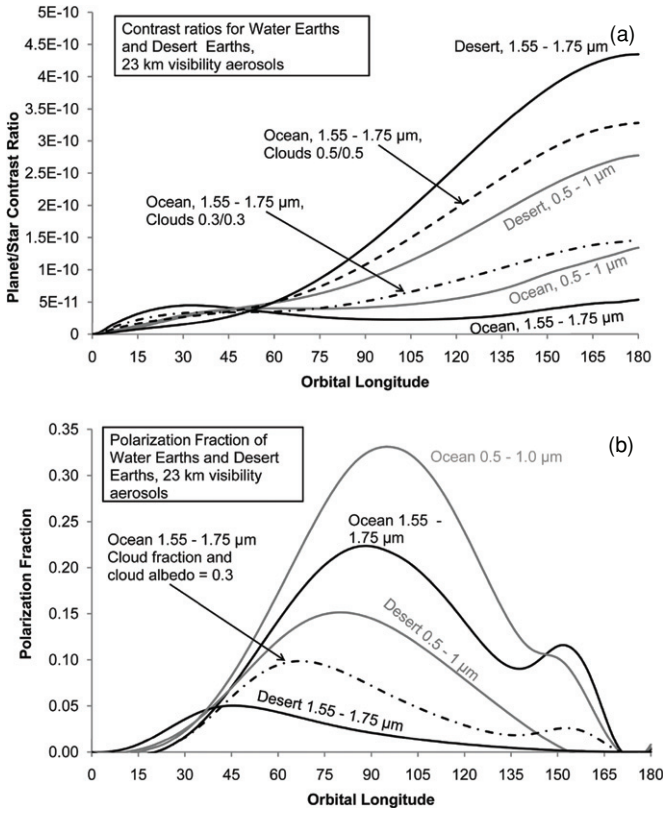

Figure 4. Contrast ratio (a) and polarization fraction (b) for water Earths and desert Earths with 23 km visibility aerosols; using NIR bands increases the difference in contrast ratio between a water Earth and a desert Earth, although clouds reduce the difference; the polarization peak at OL = 74° from an ocean is essentially undetectable for either waveband with 23 km aerosols.

Finally, we investigate whether or not observing in the NIR increases the observable difference between a water Earth and a desert Earth. In Figure 4(a), we see that the contrast ratios for desert and ocean planets with 23 km visibility aerosols, observed in the 1.55–1.75 μm window (and in the 2.1–2.3 μm waveband, not shown) are many times larger than for the same two planets observed in the 0.5–1.0 μm range. We note that Lambertian clouds with a cloud fraction of 0.5 and albedo of 0.5 (dashed curve) or 0.3 and 0.3 (dot-dashed curve) significantly reduce the difference, however.[10] In Figure 4(b), we see that the polarization fractions for both planet types are higher in the 0.5–1.0 μm window than in the 1.55–1.75 μm window; this is caused primarily by increased Rayleigh scattering from the atmosphere (and from the ocean in the water Earth case) at the shorter wavelength band. The polarization fractions for the two water Earth cases peak at 91° (0.5–1.0 μm) and 88° (1.55–1.75 μm), which in either case would not be interpreted as indicative of a water surface. Again, clouds have a significant effect, in this case reducing the polarization fraction (dot-dashed curve).

The desert Earth curves are also instructive—the polarization fraction curve of the desert Earth at 0.5–1.0 μm peaks at about 0.15 at OL = 80° and could easily be mistaken for the diluted polarization signature of a water planet. In contrast, the polarization fraction of the desert Earth observed at 1.55–1.75 μm has peak polarization fraction of only about 0.05 and peaks near 45°, so would not be misidentified as a water surface signature.

[10] As discussed in Zugger et al. (2010), cloud scattering is complex, and the variety of cloud fractions and cloud albedo among the planets in our solar system is enormous; therefore, these values of cloud fraction and cloud albedo are no more than convenient examples, and in particular we do not imply any correlation between the numerical values of cloud fraction and cloud albedo. The integrated light scattered from clouds, and therefore the cloud contribution to contrast ratio, is roughly proportional to the product of the cloud fraction and albedo.

4. DISCUSSION AND CONCLUSIONS

Our results confirm that longer wavelength NIR observations significantly reduce interference from Rayleigh scattering. The results also indicate that, at NIR wavelengths, atmospheric aerosols dominate planetary contrast ratios of water Earths, even when those aerosols are optically very thin by average Earth standards (60 km visibility). For planets with Earth-like atmospheric attenuation and Rayleigh scattering, and these very thin aerosols, observing in the 1.55–1.75 μm waveband reveals a water surface polarization signature, but observing in the 0.5–1.0 μm waveband does not. For thicker aerosols with a visibility of 23 km, still representing a clear day on Earth, the water surface glint is hidden in either waveband.

The difference in contrast ratio between a water Earth and a desert Earth, which is caused primarily by differences between desert and marine aerosols, is enhanced for the NIR bands versus the 0.5–1.0 μm waveband. Earth-like deserts could provide a polarization fraction mimicking a water surface when observed at 0.5–1.0 μm. This false positive does not occur for NIR observations—desert Earths observed in the NIR exhibit a peak polarization fraction of only about 0.05. However, Lambertian clouds on the water Earth significantly reduce the detectable differences between water and desert Earths.

Large, low noise HgCdTe and InSb detector arrays will allow ever improving observation of exoplanets at NIR wavelengths beyond the $\sim$1 μm limit of silicon arrays. However, our model shows that, even in the NIR, ocean glint signatures would be detectable only on ocean planets with very thin aerosols and little cloud cover. Also, diffraction increases with wavelength, making separation of planet and star more difficult at longer wavelengths. Therefore, we conclude that, for a space-based planet finder, the likely additional expense and reduced resolution of NIR detectors is probably not justified by the limited improvement in the chances of detecting surface oceans on water Earths. That said, NIR capability on a future planet finder mission might allow detection of absorption by gases such as CO_2 and CH_4, and additional absorption bands of water vapor, on planets similar to modern or ancient Earth (Des Marais et al. 2002). Comparison of planet/star contrast ratios in absorption bands versus window regions in the NIR may also be an effective method of detecting these gases.

The authors gratefully acknowledge the efforts of the following in funding this research: Carl Pilcher of the NASA Astrobiology Institute; Vikki Meadows of the University of Washington and the Virtual Planetary Laboratory; Nick Woolf of the University of Arizona; and the Penn State Astrobiology Research Center. The authors also thank Eric Vermote of the University of Maryland and NASA/Goddard for providing startup information on the 6SV code. The Center for Exoplanets and Habitable Worlds is supported by the Pennsylvania State University, the Eberly College of Science, and the Pennsylvania Space Grant Consortium. This work was performed under the following NASA Contracts: NNA04CC06A, NNX08A018G, and 463006 UNIWASH VPL (supported under solicitation NNH05ZDA001C).

REFERENCES

Angel, R. 2003, in Proc. Towards Other Earths: DARWIN/TPF and the Search for Extrasolar Terrestrial Planets, ed. M. Fridlund & T. Henning (ESA SP-539; Noordwijk: The Netherlands), 221

Bailey, J. 2007, Astrobiology, 7, 320

Barman, T. 2007, ApJ, 661, L191

Burriesci, L. G. 2005, Proc. SPIE, 5904, 590403-1

Cavarroc, C., & Boccaletti, A. 2006, A&A, 447, 397

Cockell, C. S., Léger, A., Fridlund, M., et al. 2009, Astrobiology, 9, 1

COESA 1962, US Standard Atmosphere (Washington, DC: US Government Printing Office)

Cowan, N. B., Agol, E., Meadows, V. S., et al. 2009, ApJ, 700, 915

D'Almeida, G. A., Koepke, P., & Shettle, E. P. 1991, Atmospheric Aerosols: Global Climatology and Radiative Characteristic (Hampton, VA: A. Deepak Pub.)

Des Marais, D. J., Harwit, M. O., Jucks, K. W., et al. 2002, Astrobiology, 2, 153

Ford, E. B., Seager, S., & Turner, E. L. 2001, Nature, 412, 885

Gilmozzi, R. 2004, Proc. SPIE, 5489, 1

Hall, D. N. B., Luppino, G., Hodapp, K. W., et al. 2004, Proc. SPIE, 5499, 1

Kaltenegger, L., Selsis, F., Fridlund, M., et al. 2010, Astrobiology, 10, 89

Kiang, N. Y., Siefert, J. L., Govindjee,, & Blankenship, R. E. 2007, Astrobiology, 7, 222

Kotchenova, S. Y., & Vermote, E. F. 2007, Appl. Opt., 46, 4455

Kotchenova, S. Y., Vermote, E. F., Matarrese, R., & Klemm, J. F. J. 2006, Appl. Opt., 45, 6762

Lenoble, J., & Brogniez, C. 1984, Beitr. Phys. Atmos., 57, 1

Levine, M., Shaklan, S., & Kasting, J., ed. 2006, JPL Document D-34923 (Pasadena, CA: NASA JPL)

McClatchey, R. A., Fenn, R. W., Selby, J. E. A., Volz, F. E., & Garing, J. S. 1972, Optical Properties of the Atmosphere (3rd ed.; Hanscom AFB, MA: Air Force Cambridge Research Labs), http://oai.dtic.mil/oai/oai?verb=getRecord&metadataPrefix=html&identifier=AD0753075

McCullough, P. R. 2006, arXiv:astro-ph/0610518

Nesher, O., Pivnik, I., Ilan, E., et al. 2009, Proc. SPIE, 7298, 72983K-1

Robinson, T. D., Meadows, V. S., & Crisp, D. 2010, ApJ, 721, L67

Russell, P., Livingston, J. M., Pueschel, R. F., et al. 1996, J. Geophys. Res., 101, 18745

Sood, A. K., Richwine, R. A., Puri, Y. R., et al. 2009, Proc. SPIE, 7298, 72983D-1

Stam, D. 2008, A&A, 482, 989

Tinetti, G., Vidal-Madjar, A., Liang, M.-C., et al. 2007, Nature, 448, 169

Vermote, E. F., Tanré, D., Deuzé, J. L., et al. 2006, Second Simulation of a Satellite Signal in the Solar Spectrum-Vector (6SV), http://6s.ltdri.org/6S_code2_thiner_stuff/6s_ltdri_org_manual.htm

Williams, D. M., & Gaidos, E. 2008, Icarus, 195, 927

Woolf, N., Smith, P., Traub, W., & Jucks, K. 2002, ApJ, 574, 430

Zugger, M. E., Kasting, J. F., Williams, D. M., Kane, T. J., & Philbrick, C. R. 2010, ApJ, 723, 1168